

PAPER • OPEN ACCESS

Theoretical modeling of charge trapping in crystalline and amorphous Al_2O_3

To cite this article: Oliver A Dicks and Alexander L Shluger 2017 *J. Phys.: Condens. Matter* **29** 314005


View the [article online](#) for updates and enhancements.

Related content

- [Modelling of electron and hole trapping in oxides](#)
A L Shluger, K P McKenna, P V Sushko et al.
- [Comparison of the electronic structure of amorphous versus crystalline indium gallium zinc oxide semiconductor: structure, tail states and strain effects](#)
A de Jamblinne de Meux, G Pourtois, J Genoe et al.
- [A mechanism for Frenkel defect creation in amorphous \$\text{SiO}_2\$ facilitated by electron injection](#)
David Z Gao, Al-Moatasem El-Sayed and Alexander L Shluger

Recent citations


- [Intrinsic electronic defects and multiple-atom processes in the oxidic semiconductor \$\text{Ga}_2\text{O}_3\$](#)
Dieter Schmeißer and Karsten Henkel
- [Intrinsic electron trapping in amorphous oxide](#)
Jack Strand et al



Contact Hiden Analytical for further details:
W www.HidenAnalytical.com
E info@hiden.co.uk


CLICK TO VIEW our product catalogue

Instruments for Advanced Science




Gas Analysis

- dynamic measurement of reaction gas streams
- catalysis and thermal analysis
- molecular beam studies
- dissolved species probes
- fermentation, environmental and ecological studies




Surface Science

- UHV-TPD
- SIMS
- end point detection in ion beam etch
- elemental imaging - surface mapping



Plasma Diagnostics

- plasma source characterization
- etch and deposition process reaction kinetic studies
- analysis of neutral and radical species



Vacuum Analysis

- partial pressure measurement and control of process gases
- reactive sputter process control
- vacuum diagnostics
- vacuum coating process monitoring

Theoretical modeling of charge trapping in crystalline and amorphous Al_2O_3

Oliver A Dicks and Alexander L Shluger

Department of Physics and Astronomy, University College London, Gower Street, London WC1E 6BT, United Kingdom

E-mail: oliver.dicks.11@ucl.ac.uk

Received 2 May 2017, revised 2 June 2017

Accepted for publication 6 June 2017

Published 6 July 2017



Abstract

The characteristics of intrinsic electron and hole trapping in crystalline and amorphous Al_2O_3 have been studied using density functional theory (DFT). Special attention was paid to enforcing the piece-wise linearity of the total energy with respect to electron number through the use of a range separated, hybrid functional PBE0-TC-LRC (Guidon *et al* 2009 *J. Chem. Theory Comput.* **5** 3010) in order to accurately model the behaviour of localized states. The tuned functional is shown to reproduce the geometric and electronic structures of the perfect crystal as well as the spectroscopic characteristics of Mg_{Al} hole centre in corundum $\alpha\text{-Al}_2\text{O}_3$. An ensemble of ten amorphous Al_2O_3 structures was generated using classical molecular dynamics and a melt and quench method and their structural characteristics compared with the experimental data. The electronic structure of amorphous systems was characterized using the inverse participation ratio method. Electrons and holes were then introduced into both crystalline and amorphous alumina structures and their properties calculated. Holes are shown to trap spontaneously in both crystalline and amorphous alumina. In the crystalline phase they localize on single O ion with the trapping energy of 0.38 eV. In amorphous phase, holes localize on two nearest neighbour oxygen sites with an average trapping energy of 1.26 eV, with hole trapping sites separated on average by about 8.0 Å. No electron trapping is observed in the material. Our results suggest that trapping of positive charge can be much more severe and stable in amorphous alumina rather than in crystalline samples.

Keywords: DFT, amorphous, alumina, Al_2O_3 , hole, polaron, Mg

(Some figures may appear in colour only in the online journal)

1. Introduction

Thin films of amorphous alumina ($\text{a-Al}_2\text{O}_3$) play a key role in the development of a wide range of applications, notably non-volatile memory [2, 3] and amorphous indium gallium zinc oxide (a-IGZO) thin film transistors [4]. With its wide band gap and dielectric constant double that of SiO_2 , Al_2O_3 is a suitable replacement as the blocking dielectric in these devices, and has also been investigated as a charge trapping layer [3] in charge trap flash memory. Charge trapping in dielectrics can be both advantageous and detrimental and

significantly affects the performance of devices. However, surprisingly little is still known about intrinsic electron and hole trapping in amorphous oxides. The aim of this work is to investigate the electron and hole trapping in the bulk of crystalline and amorphous alumina.

Self-trapped hole (STH) polarons have been theoretically predicted in crystalline $\alpha\text{-Al}_2\text{O}_3$ using both INDO [5] and DFT methods [6]. The hole polaron self-trapping energy (the energy difference between the fully delocalized and localized hole states) has been predicted using the hybrid functional HSE06 [7–8] at 0.13 eV [6]. Similarly small hole trapping energies have been predicted for many crystalline oxides, such as monoclinic ZrO_2 and HfO_2 [9, 10], BaZrO_2 [11] and several others (see e.g. [6, 12]). However, experimental verification of these predictions is often challenging and there are



Original content from this work may be used under the terms of the [Creative Commons Attribution 3.0 licence](https://creativecommons.org/licenses/by/3.0/). Any further distribution of this work must maintain attribution to the author(s) and the title of the work, journal citation and DOI.

no reliable experimental data demonstrating hole polaron formation in α -Al₂O₃.

However, the experimental data [13, 14] and recent calculations suggest that structural disorder in amorphous oxides, such as a-SiO₂ [15–17] and a-HfO₂ [18], facilitates intrinsic electron and hole trapping in much deeper states than in the corresponding crystalline phases with trapping energies of about 1.0 eV. The wide applications of amorphous Al₂O₃ films prompted us to consider whether this is the case also in these films. They have a similar O 2p nature of the top of the valence band but a different character of disorder to the amorphous SiO₂ formed by a continuous random network of SiO₄ tetrahedra. Recent spectroscopic measurements of charge trapping in thin alumina films [19] have attributed states in the band gap to intrinsic hole polaron trapping and suggested that localized O 2p⁵ states are spread throughout the band gap rather than forming a relatively narrow band discussed in amorphous SiO₂ [15, 16] and HfO₂ [18].

Scarce experimental data and lack of a general consensus on the electronic properties of a-Al₂O₃ pose significant problems for theoretical predictions of the behaviour of excess electrons and holes in this system. On one hand, predicting electron or hole localization is a well-recognized challenge for DFT (see e.g. [20–23]). On the other hand, there are no reliable models for a-Al₂O₃ structures.

In order to overcome the first problem, in this work we tuned a range separated hybrid functional PBE0-TC-LRC [1] to satisfy the Koopmans' condition and then tested it against the experimental properties of the Mg_{Al} defect in crystalline alumina. An ensemble of ten amorphous structures was generated using classical molecular dynamics and a melt and quench method and their structural characteristics compared with the experimental data. Electrons and holes were then introduced into both crystalline and amorphous alumina structures and their properties calculated. These calculations demonstrate that electrons do not trap in both crystalline and amorphous alumina. However, holes self-trap in crystalline α -alumina with trapping energies of 0.38 eV and trap at intrinsic precursor sites in amorphous alumina with average trapping energy of about 1.3 eV.

2. Methodology

Localization of a small radius polaron in the bulk crystalline phase may take place at all equivalent lattice sites with equal probability. On the other hand, in amorphous structures all sites are different and charge trapping takes place at intrinsic structural precursor sites. The concentration of such sites is system specific and is difficult to predict *a priori*. At some of these sites carriers can trap spontaneously whereas at others trapping requires overcoming an energy barrier. For example, the number of trapping sites where electrons can localize spontaneously in a-SiO₂ has been shown to be around $4 \times 10^{19} \text{ cm}^{-3}$ [17]. Therefore finding one such a site in a periodic cell requires a cell size of around 1000 atoms. Using periodic cells is required in order to avoid border effects which may affect the characteristics of trapped charges in finite systems.

Table 1. Parameters for the potential [25] used to generate the amorphous Al₂O₃ structures.

Atom	$q(e)$	$A(\text{\AA})$	$B(\text{\AA})$	$C(\text{\AA}^3 \text{ eV}^{1/2})$	$D(\text{\AA}^{-1} \text{ eV})$
Al	1.4175	0.7852	0.034	0.3816	0.04336
O	−0.9450	1.8215	0.138	0.9391	0.04336

However, this makes the amorphous structures quasi-periodic and induces constraints on the structural relaxation accompanying charge trapping. Taken together these factors imply that simulations should be performed in the largest periodic cells feasible for DFT calculations. However, different trapping sites have different trapping energies and spectroscopic characteristics. To credibly predict distributions of properties, calculations in many models are required.

2.1. Generation of the amorphous structure

In order to create sufficient statistics, ten sample structures of amorphous Al₂O₃ have been generated using a molecular dynamics (MD) melt and quench approach run using the LAMMPS code [24] and then fully relaxed using a DFT calculation described later in the paper. The MD simulation uses a 360 atom supercell of α -Al₂O₃ as the initial structure. This cell size represents a compromise between the size of the cell and computer time required to achieve representative distributions of charge trap properties. The NPT ensemble is used with a time-step of 0.1 fs. The initial structure is equilibrated at 300 K for 10 ps. The temperature is then increased to 5000 K over 20 ps. This is then followed by an equilibration at 5000 K for 20 ps. The structure is then cooled to 1 K to generate the final structure, with cooling rates of 1 K ps^{−1}, 10 K ps^{−1} and 100 K ps^{−1} being investigated.

The structural properties of the amorphous samples produced are mainly dependent on the potential used and the cooling rate of the MD simulation. The potential selected for this study has been previously used to model a-Al₂O₃ [25, 26]. It is a Born-Mayer potential with an added van der Waals term:

$$V(r_{ij}) = \frac{q_i q_j}{r_{ij}} - \frac{C_i C_j}{r_{ij}^6} + D(B_i + B_j) \exp\left(\frac{A_i + A_j - r_{ij}}{B_i + B_j}\right),$$

where the parameters for the potential are given in table 1.

2.2. DFT calculations

The electronic structure of crystalline and amorphous Al₂O₃ was calculated using the CP2K package [27]. CP2K makes use of hybrid Gaussian and plane wave type basis sets. All calculations are run at the Γ point of the Brillouin zone. The DZVP-MOLOPT-SR-GTH [28] basis sets were used for both O and Al, along with the Goedecker–Teter–Hutter (GTH) pseudopotentials [29, 30]. The converged plane wave energy cutoff was set to 500 Ry and the SCF convergence criterion was set to a maximum energy difference of 10^{-6} a.u. between steps. All final geometry relaxations were performed using the PBE0-TC-LRC [1] hybrid functional described below and used the conjugate gradient optimizer with a maximum

force convergence criterion of $0.05 \text{ eV } \text{\AA}^{-1}$ for each atom. The auxiliary density matrix method [31] (ADMM) was used to reduce the computational cost associated with using the range separated hybrid functional, allowing the calculation of relatively large 360 atom systems.

2.2.1. Tuning the functional. As noted above, self-trapped polarons in crystals usually have small trapping energies of the order of $0.1\text{--}0.3 \text{ eV}$. This means that even qualitative predictions of their stability are greatly affected by the choice of the Hamiltonian. The early many-electron calculations of polarons and excitons in insulators were carried out using the Hartree–Fock method (e.g. [32, 33]) and semi-empirical quantum chemistry techniques (e.g. [34, 35]), which tend to over-localize electronic states. This is not a big problem for e.g. calculating the spectroscopic properties of well localized polarons. However, predicting the formation and stability of polaronic states remains a challenge. It has been realized early on that DFT in LDA and GGA approximations tends to delocalize electrons and fails to predict exciton [21] and hole polaron [20] localization in the well-established cases. This has been attributed to the self-interaction error [20, 21] and a quick fix of adjusting the amount of Hartree–Fock exchange in hybrid density functionals has been widely implemented to provide the electron localization in known cases (e.g. [15, 20, 36]). A cheaper and more targeted approach is to adjust the U parameter in LDA+ U or GGA+ U calculations of polaron states. Several flavours of this approach have been suggested over the years, as discussed in [37–40], and it is still very widely used. The predictive power of these two approaches is again limited but they can be used very effectively in ‘test and predict’ mode where the parameters (e.g. the amount of HF exchange or the U value) are first fitted to reproduce the established data and then the same parameters are used for predictive calculations. However, the transferability of these parameters between materials is quite limited.

It has been noted more generally [23, 41] that failures of DFT to correctly predict localization of electronic states and charge transfer spectra are associated with a wrong asymptotic behaviour of approximate exchange–correlation (XC) potentials for isolated molecules, ‘nearsightedness’ of XC response kernels, and lack of the integer discontinuity [41]. Therefore significant recent efforts have focused on creating so called Koopman’s-compliant exchange–correlation functionals with piecewise linearity with respect to fractional particle occupations and developing range-separated hybrid functionals for molecular systems [39, 42–44]. A commonly used method is to correct the non-piecewise linearity of the total energy (E) with respect to (the continuous) electron particle number (N) in DFT systems [39, 42]. The linearity condition, where $(d^2E/dN^2 = 0)$, is shown to be a property of the exact exchange–correlation functional by Perdew *et al* [45]. Local and semi local functionals deviate from the straight line behaviour, instead showing curvature where $(d^2E/dN^2 > 0)$, while in HF theory the opposite behaviour is observed and $(d^2E/dN^2 < 0)$. Lany and Zunger [39] proposed that, by enforcing the linearity condition, the energy of the

self-interaction of the electron or hole after addition is cancelled by the energy of the wavefunction relaxation, allowing a more accurate description of localized states. Thus by either applying DFT+ U [39] or the use of hybrid functionals [42], the linearity condition can be enforced. It has not been demonstrated that satisfying this condition is necessary for correct description of electron localization. However, it has been observed that localization can indeed be achieved by tuning the parameters of the effective localizing potential [39] to satisfy the linearity condition.

In an alternative approach [43, 46], range separated hybrid functionals are investigated, with parameters optimally tuned so that the generalized Koopmans’ condition is enforced, equivalent to ensuring the linearity condition as in the methods mentioned above. This enables quantitative predictions of band gaps and energy levels in molecules to be made without the need for empirical matching. This approach, however, cannot be easily generalized for infinite solids [47].

In this paper we test a similar approach where the range separated hybrid functional PBE0-TC-LRC [1] is used with a tuned cutoff radius. This functional has been introduced to allow efficient calculation of exact exchange in Γ point codes, such as CP2K, and provides large speedup of the calculations without loss of accuracy. The exchange–correlation part of the PBE0-TC-LRC functional has the form

$$E_{xc} = aE_x^{\text{HF,TC}} + aE_x^{\text{PBE,LRC}} + (1-a)E_x^{\text{PBE}} + E_c^{\text{PBE}}.$$

PBE0 is the standard PBE hybrid functional [48, 49] with $a = 0.25$. $E_x^{\text{HF,TC}}$ is the truncated Hartree–Fock exchange, $E_x^{\text{PBE,LRC}}$ is the long range PBE exchange with a truncated Coulomb potential, E_x^{PBE} is the PBE exchange and E_c^{PBE} is the PBE correlation. The truncated Coulomb (TC) version of the Hartree–Fock exchange takes the form

$$E_x^{\text{HF,TC}} = -\frac{1}{2} \sum_{ij} \iint \psi_i(r_1) \psi_j(r_1) g_{ic}(r_{12}) \times \psi_i(r_2) \psi_j(r_2) d^3r_1 d^3r_2 \quad (1)$$

where the operator

$$g_{ic}(r_{12}) = \begin{cases} \frac{1}{r_{12}} & \text{for } r_{12} < R \\ 0 & \text{for } r_{12} > R \end{cases} \quad (2)$$

where R is the cutoff parameter. The long-range correction (LRC) is based on the PBE exchange hole [1]. This functional is similar to HSE06 [7–8] in that, unlike many other range-separated hybrid functionals, it uses short-range exact exchange and a long-range semi-local functional.

We use the cutoff radius R as a variational parameter which is tuned to minimize a deviation of the functional from straight line behaviour, unlike e.g. in previous work [42], where the proportion of exact exchange, a was varied, though both change the contribution of the exact exchange to the energy (see also [44]).

To find the cutoff parameter, R , we use the same method as in [43, 44]. The exact form of Koopmans’ Theorem in K–S theory:

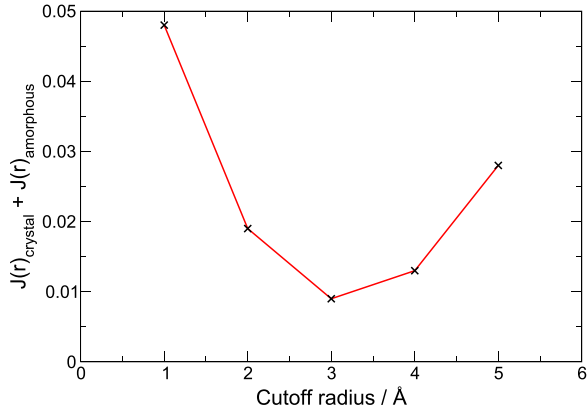


Figure 1. The total of the $J(R)$ functions of both the amorphous and crystalline structures plotted against the PBE0-TC-LRC cutoff radius. It can be seen that the error is at a minimum when $R = 3.0$ Å.

$$\varepsilon_{\text{HOMO}}(N) = -I(N)$$

where $\varepsilon_{\text{HOMO}}(N)$ is the energy of the K–S highest occupied molecular orbital (HOMO) and $I(N)$ is the ionization potential of the N electron system. The ionization potential of the N electron system can also be defined;

$$I(N) \equiv E_{\text{gs}}(N-1) - E_{\text{gs}}(N),$$

the difference between the energy of the ground state of the $N-1$ electron, $E_{\text{gs}}(N-1)$, and N electron, $E_{\text{gs}}(N)$ system, or the energy to remove an electron from the system. A similar condition can be imposed for the addition of an electron to the system, where the LUMO energy is equated with the electron affinity. From these equations R can then be tuned so that the function [46]

$$J(R) = [\varepsilon_{\text{HOMO}}^R(N) + I^R(N)]^2 + [\varepsilon_{\text{HOMO}}^R(N+1) + I^R(N+1)]^2 \quad (3)$$

is minimized. This equation also accounts for the error in the LUMO level, or the $N+1$ system, important when investigating the possible localization of electrons. We apply this functional in the ‘test and predict’ manner where the functional is first tested using the data available for crystalline alumina and then used to make predictions for the amorphous structure.

As one can see in figure 1, the deviation of straight line error (DSLE) is minimized when $R = 3.0$ Å. At this cutoff the largest absolute error in fulfilling the Koopman’s condition is 0.04 eV. It is significantly smaller than the trapping energies and therefore may allow qualitatively accurate predictions of the properties of trapped holes and electrons in both crystalline and amorphous alumina.

3. Results of calculations

3.1. Properties of α -Al₂O₃

The tuned PBE0-TC-LRC [1] functional was benchmarked against known structural and electronic properties of the crystalline system. The structural properties of the 360 atom

Table 2. Comparison of the calculated lattice parameters for corundum α -Al₂O₃ with the experimental data [50].

Lattice parameter	Theory (Å)	Experiment (Å)	Error (%)
a	4.7555	4.7605	−0.1
b	8.2370	8.2454	−0.1
c	12.9730	12.9956	−0.2

Table 3. Comparison of the properties of the crystalline, α -Al₂O₃, system calculated using the HSE06 [7] functional and PBE0-TC-LRC [1] functionals with a varied cutoff.

Functional	Maximum DSLE (eV)	Kohn–Sham Bandgap (eV)	Hole E_{trap} (eV)
HSE06 [7]	0.04	8.1	0.13
PBE0-TC-LRC	0.04	8.6	0.38
$R = 3.0$			
PBE0-TC-LRC	0.10	8.7	0.42
$R = 5.0$			

α -Al₂O₃ cell were in good agreement with x-ray crystallography data [50] (see table 2), with all the calculated lattice parameters within 0.2% of the experimental values after a full cell relaxation.

It is also important that the functional reproduces the bulk electronic structure. The K–S band gap was calculated to be 8.6 eV (see table 3), which is close to the experimental optical band gap of 8.8 eV [51]. It should be noted that the functional was tuned to obey the Koopmans’ condition rather than fit to empirically match the experimental optical band gap. The electronic structure was also calculated using the HSE06 [7] and the PBE0-TC-LRC functional with a larger cutoff of 5.0 Å (see table 3). It can be seen that HSE06, whilst having a similar DSLE, underestimates the band gap by approximately 0.8 eV.

3.1.1. Properties of Mg_{Al} defect. Due to low trapping energies, it is difficult to measure the properties of self-trapped hole polarons in α -Al₂O₃ experimentally. Instead the functional can be benchmarked against the EPR [52, 53] and optical absorption [54] properties of the Mg_{Al} defect. It has originally been assumed that Mg acts as an acceptor [55], with the hole localizing on the nearest neighbour oxygen, becoming O[−], which makes it a good test system for hole trapping. However, previous INDO calculations [5] suggested the hole localization over two O ions is more energetically favourable.

The calculations performed in this paper show that the compensating hole localizes predominantly on one O ion (a spin of 0.76 from Mulliken analysis), as can be seen in figure 2. This localization is accompanied by a large elongation of the Mg–O bonds by 0.4 Å from the original perfect lattice positions. The three nearest neighbour Al ions that lie in the same plane as the O[−] displace away from the O atom by less than 0.1 Å (see table 4). The calculated isotropic hyperfine splitting for these nearest neighbour Al are shown in table 4 and are compared to the experimental ENDOR measurements [53]. These results agree well with the experimental results and also agree qualitatively with Adrian *et al* [55] whose semi-empirical model

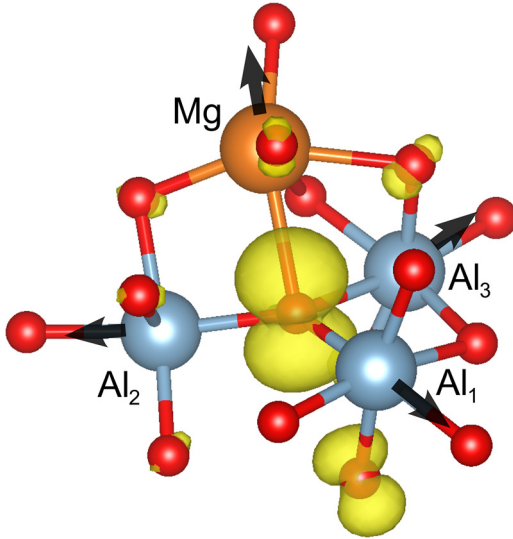


Figure 2. The spin density of the Mg_{Al} defect, where the hole is predominantly localized on one O ion. Mg is brown, O red and Al blue. The arrows show the direction of cation relaxation.

Table 4. The calculated isotropic hyperfine parameters of the Mg_{Al} defect as well as the experimental ENDOR values [53]. It also shows the nearest neighbour distances to the oxygen where the hole localizes and compares them to the original predictions from theory [55]. The atom labels are from figure 2.

Atom X	Isotropic hyperfine (MHz)		O–X distance (Å)	
	Calc.	Exp. [53]	Calc.	[55]
Al ₁	18.91	19.03	1.888	1.834
Al ₂	13.85	14.18	1.942	1.917
Al ₃	9.12	7.29	2.062	2.104
Mg	2.06	—	2.353	—

of the defect predicts a strong dependence of the hyperfine constant on the O–Al distance. It also serves to confirm that a single O traps a hole when an Mg_{Al} defect is introduced, and is able to predict the structural relaxation of that site.

The unoccupied K–S LUMO energy level of the Mg_{Al} defect lies 2.15 eV above the VBM. Time-dependent DFT (TD-DFT) calculations [56] of the optical absorption of this defect demonstrate broad spectrum with the maximum at 2.4 eV determined by transitions from the valence band states into the LUMO state. This can be compared with the optical absorption spectrum reported by Wang *et al* [54] which has a maximum at 2.6 eV with a full width half maximum of 1.3 eV that they associate with the Mg_{Al} defect. This assignment is confirmed by ESR measurements.

These results demonstrate that the tuned PBE0-TC-LRC functional performs well for perfect crystalline alumina and also allows positive identification of the Mg_{Al} defect in $\alpha\text{-Al}_2\text{O}_3$. This gives confidence to consider intrinsic polarons in crystalline and amorphous alumina.

3.2. The hole polaron in $\alpha\text{-Al}_2\text{O}_3$

Intrinsic hole polarons in crystalline $\alpha\text{-Al}_2\text{O}_3$ have been studied theoretically using classical and INDO methods [5].

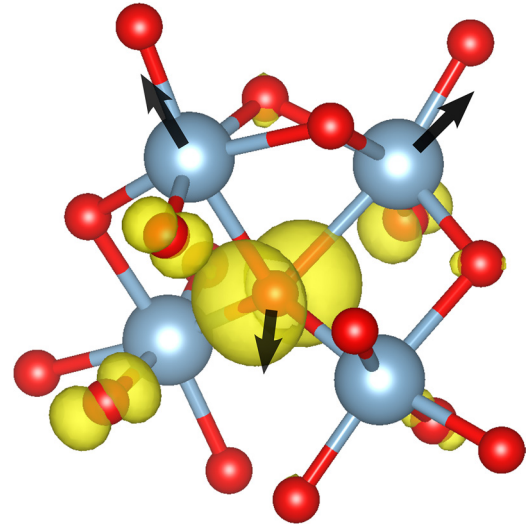


Figure 3. The spin density of the hole polaron in $\alpha\text{-Al}_2\text{O}_3$, and the direction of relaxation of the ions. The Al ions are coloured blue and the O are red.

Zhukovskii *et al* [5] investigated whether STH polarons are more stable when localized on a single O or over two O ions, concluding that two-site holes are more stable. They calculated trapping energies to characterize the stability of the holes, however, the INDO method leads to a large over-estimation of these energies, in the order of 3–5 eV. The trapping energy, E_{trap} , is defined as

$$E_{\text{trap}} = E_{\text{neutral}}(N - 1) - E_{\text{polaron}}(N - 1)$$

where $E_{\text{neutral}}(N - 1)$ is the total energy of the unrelaxed cell in the neutral geometry with a delocalized hole in the valence band and $E_{\text{polaron}}(N - 1)$ is the total energy of the fully relaxed cell with a hole polaron. The same definition is used in this paper and is comparable to the trapping energies calculated in previous papers [5, 6].

More recently, DFT calculations using HSE06 [7] have calculated the trapping energy of hole polarons to be 0.13 eV [6], with the majority of the spin density located on a single oxygen. This result is reproduced in this paper using the HSE06 functional (see table 3).

The calculations performed in this paper using the tuned PBE0-TC-LRC functional predict that introduction of a hole to the system results in self-trapping, with 0.8 of the spin (from Mulliken analysis) localized on one O ion (see figure 3). The calculated trapping energy of the hole polaron in $\alpha\text{-Al}_2\text{O}_3$ is 0.38 eV. Hole localization is accompanied by displacements of the surrounding ions, with three of the four Al–O bonds elongating by approximately 0.1 Å, and the elongation of one Al–O bond by 0.3 Å. The top of the valence band of $\alpha\text{-Al}_2\text{O}_3$ is composed of O 2p orbitals. The dispersion of this band is small, meaning that the increase in kinetic energy of the hole upon localization is smaller than the energy of the lattice relaxation, resulting in the high trapping energies. The calculated trapping energy is larger than that using HSE06 calculated here and in previous papers [6], likely because the functional more strongly localizes the hole, and includes a larger contribution of exact exchange than HSE06. It can

Table 5. Densities of α - Al_2O_3 measured using a variety of experimental techniques and compared to the average density calculated using DFT in this paper.

Authors	Growth technique	Substrate	Measuring technique	Density (g cm ⁻³)
Groner <i>et al</i> [57]	ALD(306 K)	n-type Si	XRR	2.46
	ALD(450 K)	n-type Si	XRR	3.06
Ilic <i>et al</i> [58]	ALD	Si	NEMS	3.20
Ok <i>et al</i> [4]	ALD	SiN _x	XRR	2.97–3.14
PBE0-TC-LRC				3.14

be seen from table 3 that HSE06 does not perform as well as PBE0-TC-LRC in reproducing the correct band gap which could be a result of the over delocalization.

3.3. The geometric structure of α - Al_2O_3

To study polarons in amorphous alumina, the geometric structures used for calculations have to accurately reproduce the overall topology and local features of the material. The geometric properties of the ten α - Al_2O_3 structures generated in this study through MD melt-quench show excellent agreement with experimentally measured densities, coordination numbers and x-ray diffraction data of lab grown thin films. After the structures were generated using MD melt-quench procedure, a full cell optimization was performed using the PBE functional. A final geometry optimization was then performed using the tuned PBE0-TC-LRC [1] functional.

The density of α - Al_2O_3 (a crystalline phase) is 3.95 g cm⁻³, but when thin films of amorphous alumina are grown large changes in the density of the material are detected (see table 5). Groner *et al* [57] deposited thin films of alumina at varying low temperatures using ALD on n-type silicon wafers and quartz crystal microbalance (QCM) substrates. The QCM was used to measure the mass of a film whilst various other measurement techniques were used to determine the thickness including AFM and spectroscopic ellipsometry. X-ray reflectivity (XRR) was also used independently to determine the density. These different measurement techniques gave a range of values for the density but most methods were within 0.1 g cm⁻³ of each other. The average reported densities were 3.0 g cm⁻³ for films grown at 177 °C and 2.5 g cm⁻³ for those grown at 33 °C. Measurements of alumina film density performed by Ilic *et al* [58] on ALD ultrathin films using nano-mechanical oscillators give a value of 3.2 ± 0.1 g cm⁻³. The densities of the generated structures of α - Al_2O_3 agree very well with the experimental values, with the averages lying within the range of 3.06–3.25 g cm⁻³ (see table 5).

The radial distribution functions (RDFs) of the amorphous structures, shown in figure 4, agree well with the x-ray and neutron diffraction studies performed by Lamparter [59], with the peak maxima within 0.05 Å of the experimental results. The RDFs were scaled so that the maximum peak intensities were equal, but no other fitting was carried out. Lee *et al* [60] use 2D 3QMAS NMR to measure coordination numbers of ions in thin films of Al_2O_3 deposited on Si(100) wafers by RF magnetron sputtering at low temperatures. They measure the distribution of coordination numbers of Al with O to be

^[4]Al 55% \pm 3%; ^[5]Al 42% \pm 3%; ^[6]Al 3% \pm 2%, compared to an average of 53%, 37% and 10% from the ten generated amorphous structures respectively. This shows that in amorphous films most Al are under-coordinated with respect to α - Al_2O_3 , where all Al are 6-coordinated with O.

3.4. The electronic structure of α - Al_2O_3

3.4.1. Bulk structure. Having demonstrated that the tuned density functional gives good agreement with the experimental data for α - Al_2O_3 and the structure of α - Al_2O_3 , we now turn to the electronic structure of α - Al_2O_3 . The average Kohn–Sham band gap is calculated to be 5.5 eV from the 10 α - Al_2O_3 structures. Experimentally the band gap has been measured to be 6.0–7.1 eV [61–65], though often tails are observed in the spectra which are most likely due to localized states at band edges. The electronic structure of amorphous solids can be further characterized using the inverse participation ratio (IPR). This method takes advantage of the atom centered basis set used in CP2K to quantify the degree of localization of each eigenvector. It has often been used to characterize localization of vibrational and electronic states in amorphous solids [66–70]. The IPR is defined as:

$$\text{IPR}(\psi_n) = \frac{\sum_{i=1}^N a_{ni}^4}{(\sum_{i=1}^N a_{ni}^2)^2}$$

where

$$\psi_n = \sum_{i=1}^N a_{ni} \phi_i$$

is the n th Kohn–Sham eigenvector (MO), N is the number of atomic orbitals and ϕ_i is the i th atomic orbital. The IPR is $1/N$ for completely delocalized MOs, and 1 for MOs that are localized on a single atomic basis orbital.

The IPR analysis of α - Al_2O_3 , shown in figure 5(b), demonstrates that there are many localized states at the top of the valence band but the bottom of the conduction band is formed by delocalized states. Crucially, the states in the valence band only become completely delocalized approximately 1.0 eV below the HOMO, and can be attributed to the onset of the mobility edge. The mobility edge is usually defined as a transition between localized states, which do not contribute to the electrical conductivity of the system, and extended states, which can contribute to the electrical conductivity in disordered systems [71]. Using the IPR analysis, one can approximately define mobility edge as the onset of states with an IPR

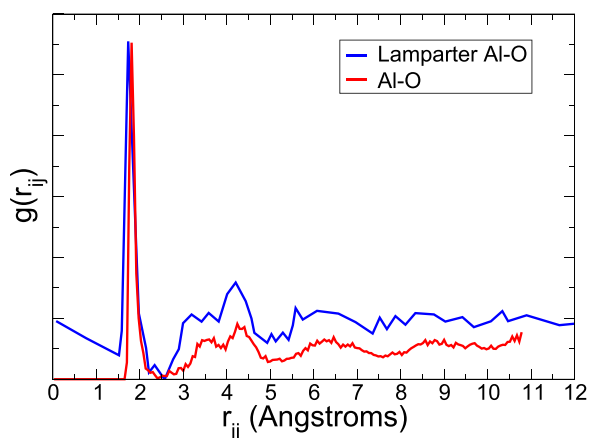


Figure 4. Comparison of the calculated and experimental [59] radial distribution function for Al–O coordination.

corresponding to delocalized states [68, 70, 72]. This suggests that the HOMO-LUMO gap is not a good approximation of the band gap in amorphous materials, and that the band gap will rely on the position of the mobility edge. This would place the predicted band gap in the 6.0–7.0 eV range. A recent paper [19] reports a band gap of 7.1 eV from EELS measurements, but also show non-zero scattering intensity to below 6 eV, in agreement with the calculations presented in this paper.

The degree of electron localization at the band edges is most likely due to the respective orbital character of the valence and conduction bands. The density of states in figure 5(a) shows that the top of the valence band is composed of O 2*p* orbitals, whereas the bottom of the conduction band is composed predominantly of Al 3*s* orbitals. These states demonstrate a very high dispersion in crystalline corundum structures [73] which projects into the *a*-Al₂O₃ states in terms of band unfolding procedure [74]. The high electron mobility prevents localization at the bottom of the conduction band.

3.4.2. Hole polarons in *a*-Al₂O₃. The states with high localization at the top of the valence band (figure 5(b)) in the neutral system correspond with local structural features that result in hole trapping, defined as ‘precursor sites’ for the purposes of this paper. When a hole is introduced to the system it will spontaneously localize at one of the precursor sites predicted from the IPR. In all ten amorphous structures of Al₂O₃ strong intrinsic hole trapping is observed, with an average trapping energy of 1.26 eV. The range of trapping energies is calculated to be 1.0–1.5 eV (see table 6). The much larger trapping energies observed in the amorphous structures when compared to the crystalline is most likely due to the under-coordination of the O atoms, where over 80% are 3-coordinated with Al, rather than 4-coordinated as in α -Al₂O₃. This under coordination leads to much larger relaxations of the ions and a different configuration of the trapped hole polaron. Many of the precursor sites where the hole polarons are able to localize include a 2-coordinated O ion (see table 6), which account for approximately 5% of oxygens in the amorphous structure, though not all precursor sites include a 2-coordinated oxygen.

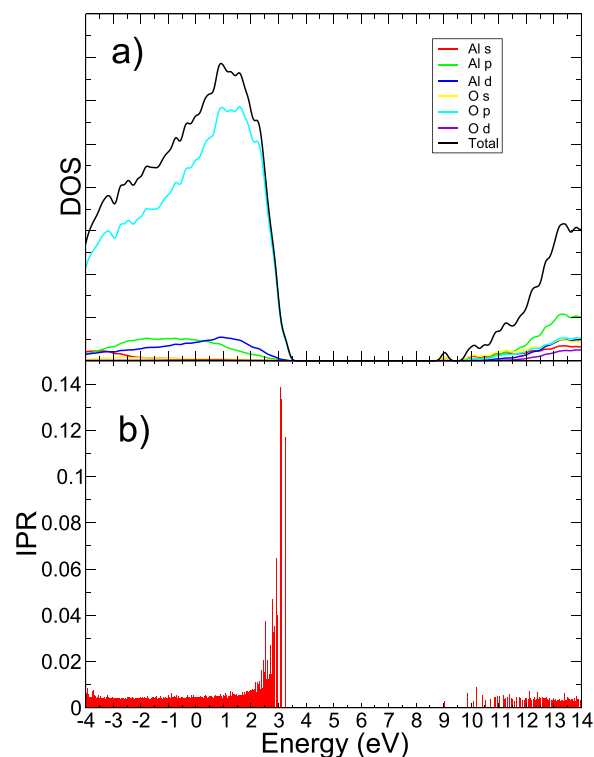


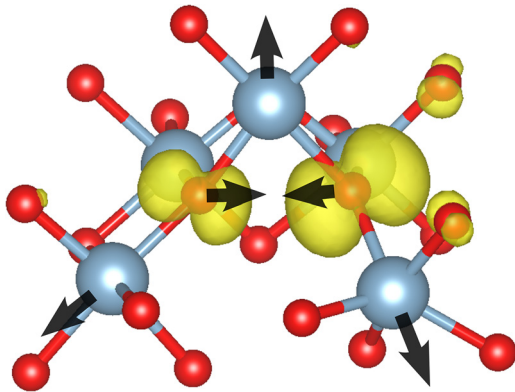
Figure 5. (a) The projected density of states (PDOS) and (b) inverse participation ratio (IPR) of one structure of *a*-Al₂O₃, showing strong localization of the top of the valence band.

Although the precursor sites are most easily identified from the IPR data, there are structural similarities between the hole traps. Unlike in α -Al₂O₃ where the hole localizes on one O ion, in *a*-Al₂O₃ over 90% of the spin density localizes on two nearest neighbour O ions (see figure 6) with an average O–O separation of 2.6 Å before relaxation (see table 6). This means the hole traps have a local structure involving multiple ions. The spin density is not, however, evenly distributed between the two oxygens, one normally accounts for 0.7 of the spin (from Mulliken analysis) with the other approximately 0.2. Between the two O ions where the hole is localized there is a large contraction of the O–O bond of 0.3–0.4 Å, much larger than the relaxation of the O–O bonds in the crystalline system which are less than 0.1 Å. The O–Al–O bond angle also decreases by an average of 10°. There is also a small displacement of the Al ions, which move approximately 0.1 Å.

Due to the large distribution of bond angles and bond distances in *a*-Al₂O₃ there are multiple precursor sites where the local structural configuration of the ions allows for hole trapping. These precursor sites are identified using the IPR data, and hole polarons can be localized at different sites within the cell. In *a*-Al₂O₃ there are an average of three to four precursor sites per 360 atom cell where hole polarons are able to trap, with an average separation of 8 Å between sites. This leads to a maximum density of precursor sites of approximately $2.6 \times 10^{20} \text{ cm}^{-3}$. The variation of trapping energies of the precursor sites within the cell is similar to that between different samples, with a typical variation of 0.3 eV.

Table 6. The properties of different hole trapping sites in the ten geometry samples of a- Al_2O_3 , including the coordination number of the oxygen where the majority of the spin is localized.

Sample	Trapping energy (eV)	Unrelaxed O–O distance (Å)	Relaxed O–O distance (Å)	O coordination number
1	1.16	2.61	2.23	2
2	1.00	2.61	2.39	3
3	1.39	2.55	2.37	3
4	1.49	2.68	2.12	2
5	1.32	2.46	2.47	2
6	1.10	2.91	2.61	2
7	1.34	2.41	2.10	3
8	1.42	2.65	2.53	2
9	1.08	2.69	2.59	2
10	1.29	2.69	2.39	2

**Figure 6.** The spin density of the hole polaron in a- Al_2O_3 , and the direction of relaxation of the ions. The Al ions are coloured blue and the O are red.

Using a nudged elastic band calculation (NEB) the thermal barrier to a hole hopping between two hole trapping sites in the same cell was calculated to be 0.3–0.6 eV. However, unlike in crystalline Al_2O_3 where adjacent hole trapping sites are equivalent, in the amorphous material precursor sites are separated by distances of 8.0 Å, which would suggest that transport is more likely to be through a tunneling process. The high trapping energies of hole polarons and barriers to hopping also suggest that there is likely to be stronger positive charging in a- Al_2O_3 than in the crystalline material, and that this charging could be due to intrinsic hole trapping rather than impurities in the material.

3.4.3. Electron trapping in Al_2O_3 . Self trapped electron polarons in crystalline $\alpha\text{-Al}_2\text{O}_3$ were not found to be stable. This is most likely, as stated earlier, due to the large dispersion of the conduction band at the Γ -point of $\alpha\text{-Al}_2\text{O}_3$ [73], the small relaxation of the lattice cannot compensate for the large increase in kinetic energy of the electron as it is localized and so the polaron is not self trapped.

Although deep electron traps in a- Al_2O_3 have been observed experimentally [2], after examining 30 different geometric structures (20 of them 120 atom models) no significant evidence for intrinsic electron trapping was observed. Extra electrons are delocalized at the bottom of the conduction band. The IPR of a- Al_2O_3 in figure 5(b) suggests the reason for the much lower density of electron traps when

compared to hole traps is there are no localized precursor sites at the bottom of the conduction band. In materials which show strong intrinsic electron trapping, the bottom of the conduction band generally has lower dispersion and is composed of orbitals that are more directional. In the case of HfO_2 [18], the CBM is composed of d orbitals and demonstrates electron trapping energies of 1.4 eV, and even the formation of electron bipolarons. In a-Se photodetectors [75] it is reported that an a- HfO_2 blocking layer is more effective at suppressing both electron and hole injection than an a- Al_2O_3 layer. The greater number of charge traps in HfO_2 could suggest that while pure alumina does trap charge, it only traps holes.

4. Conclusions

We have studied intrinsic charge trapping in amorphous alumina through the use of DFT simulations with the range-separated hybrid functional PBE0-TC-LRC. The truncation radius was tuned to provide the piece-wise linearity of the energy. Satisfying this condition led to qualitatively correct predictions of electron and hole localization at impurities in other calculations [39, 42]. The performance of PBE0-TC-LRC with $R = 3.0$ Å was tested by reproducing the properties of $\alpha\text{-Al}_2\text{O}_3$ as well as the spectroscopic properties of the Mg_{Al} defect in $\alpha\text{-Al}_2\text{O}_3$. The substitution of Al by Mg in $\alpha\text{-Al}_2\text{O}_3$ creates a local negative charge which is known to be compensated by positive hole trapped on a nearby O ion. This defect has been studied by EPR [52, 53] and optical spectroscopy [54].

The calculations reproduce the structure and the band gap of $\alpha\text{-Al}_2\text{O}_3$ as well as the spectroscopic properties of Mg_{Al} defect in good agreement with the experiment. Using this functional, it was shown that holes can trap spontaneously in amorphous alumina on two nearest neighbour oxygen sites, with an average trapping energy of 1.26 eV. It is also demonstrated that there is a high density of hole trapping precursor sites in a- Al_2O_3 . These are typically low-coordinated O sites which are separated on average by about 8.0 Å. However, unlike in other oxides, such as SiO_2 and HfO_2 , no electron trapping was observed in both crystalline and amorphous alumina. This is attributed to the orbital nature of the bands, with the CBM being composed of highly dispersed $3s$ states. This suggests that the nature of intrinsic

trapping in metal oxides could be predicted by examining the fundamental orbital character of the ions in the system and the composition of the bands. These results predict that the trapping of positive charge can be much more severe and stable in amorphous alumina rather than in crystalline samples.

Acknowledgments

OAD acknowledges Argonne National Laboratory, USA for financial support. ALS acknowledges funding provided by EPSRC under grant EP/K01739X/1. Computer facilities on Archer service have been provided via the UKs HPC Materials Chemistry Consortium (EPSRC Grant No. EP/L000202). The authors wish to thank A-M El-Sayed, D Z Gao and J Strand for helpful discussions.

References

- [1] Guidon M, Hutter J and VandeVondele J 2009 *J. Chem. Theory Comput.* **5** 3010
- [2] Zahid M B, Aguado D R, Degraeve R, Wang W C, Govoreanu B, Toledano-Luque M, Afanasev V V and Van Houdt J 2010 *IEEE Trans. Electron Dev.* **57** 2907
- [3] Li Y *et al* 2015 *IEEE Trans. Electron Dev.* **62** 1184
- [4] Ok K-C, Oh S, Jeong H-J, Bae J U and Park J-S 2015 *IEEE Electron Dev. Lett.* **36** 917
- [5] Zhukovskii Y F, Kotomin E A, Nieminen R M and Stashans A 1997 *Comput. Mater. Sci.* **7** 285
- [6] Varley J B, Janotti A, Franchini C and Van de Walle C G 2012 *Phys. Rev. B* **85** 081109
- [7] Heyd J, Scuseria G E and Ernzerhof M 2003 *J. Chem. Phys.* **118** 8207
- [8] Krukau A V, Vydrov O A, Izmaylov A F and Scuseria G E 2006 *J. Chem. Phys.* **125** 224106
- [9] Muñoz Ramo D, Shluger A L, Gavartin J L and Bersuker G 2007 *Phys. Rev. Lett.* **99** 155504
- [10] McKenna K P, Wolf M J, Shluger A L, Lany S and Zunger A 2012 *Phys. Rev. Lett.* **108** 116403
- [11] Lindman A, Erhart P and Wahnström G 2016 *Phys. Rev. B* **94** 075204
- [12] Rettie A J E, Chemelewski W D, Emin D and Mullins C B 2016 *J. Phys. Chem. Lett.* **7** 471
- [13] Griscom D L 2006 *J. Non-Cryst. Solids* **352** 2601
- [14] Cerbu F *et al* 2016 *Appl. Phys. Lett.* **108** 222901
- [15] Kimmel A V, Sushko P V and Shluger A L 2007 *J. Non-Cryst. Solids* **353** 599
- [16] Farnesi Camellone M, Kühne T D and Passerone D 2009 *Phys. Rev. B* **80** 033203
- [17] El-Sayed A-M, Watkins M B, Afanas'ev V V and Shluger A L 2014 *Phys. Rev. B* **89** 125201
- [18] Kaviani M, Strand J, Afanas'ev V V and Shluger A L 2016 *Phys. Rev. B* **94** 020103(R)
- [19] Henkel K, Kot M and Schmeißer D 2017 *J. Vac. Sci. Technol. A* **35** 01B125
- [20] Lægsgaard J and Stokbro K 2001 *Phys. Rev. Lett.* **86** 2834
- [21] Pacchioni G, Frigoli F and Ricci D 2000 *Phys. Rev. B* **63** 054102
- [22] Gavartin J, Sushko P and Shluger A 2003 *Phys. Rev. B* **67** 035108
- [23] Cohen A J, Mori-Sanchez P and Yang W 2012 *Chem. Rev.* **112** 289
- [24] Plimpton S 1995 *J. Comput. Phys.* **117** 1
- [25] Bläckberg L, Metsanurk E, Tamm A, Aabloo A and Klintonberg M 2014 *Nucl. Instrum. Methods Phys. Res. A* **759** 10
- [26] Gutiérrez G and Johansson B 2002 *Phys. Rev. B* **65** 104202
- [27] VandeVondele J, Krack M, Mohamed F, Parrinello M, Chassaing T and Hutter J 2005 *Comput. Phys. Commun.* **167** 103
- [28] VandeVondele J and Hutter J 2007 *J. Chem. Phys.* **127** 114105
- [29] Goedecker S, Teter M and Hutter J 1996 *Phys. Rev. B* **54** 1703
- [30] Hartwigsen C, Goedecker S and Hutter J 1998 *Phys. Rev. B* **58** 3641
- [31] Guidon M, Hutter J and VandeVondele J 2010 *J. Chem. Theory Comput.* **6** 2348
- [32] Shluger A L, Puchin V E, Suzuki T, Tanimura K and Itoh N 1995 *Phys. Rev. B* **52** 4017
- [33] Fisher A J, Hayes W and Stoneham A M 1990 *J. Phys.: Condens. Matter* **2** 6707
- [34] Shluger A L, Kotomin E A and Kantorovich L N 1986 *J. Phys. C: Solid State Phys.* **19** 4183
- [35] Shluger A L, Heifets E N, Gale J D and Catlow C R A 1992 *J. Phys.: Condens. Matter* **4** 5711
- [36] Siculo S, Palma G, Di Valentin C and Pacchioni G 2007 *Phys. Rev. B* **76** 075121
- [37] Maxisch T, Zhou F and Ceder G 2006 *Phys. Rev. B* **73** 104301
- [38] Deskins N and Dupuis M 2007 *Phys. Rev. B* **75** 1
- [39] Lany S and Zunger A 2009 *Phys. Rev. B* **80** 085202
- [40] Erhart P, Klein A, Åberg D and Sadigh B 2014 *Phys. Rev. B* **90** 035204
- [41] Perdew J P, Ruzsinszky A, Constantin L A, Sun J and Csonka G I 2009 *J. Chem. Theory Comput.* **5** 902
- [42] Atalla V, Zhang I Y, Hofmann O T, Ren X, Rinke P and Scheffler M 2016 *Phys. Rev. B* **94** 035140
- [43] Karolewski A, Kronik L and Kümmel S 2013 *J. Chem. Phys.* **138** 204115
- [44] Autschbach J and Srebro M 2014 *Acc. Chem. Res.* **47** 2592
- [45] Perdew J P, Parr R G, Levy M and Balduz J L 1982 *Phys. Rev. Lett.* **49** 1691
- [46] Kronik L, Stein T, Refaely-Abramson S and Baer R 2012 *J. Chem. Theory Comput.* **8** 1515
- [47] Vlček V, Eisenberg H R, Steinle-Neumann G, Kronik L and Baer R 2015 *J. Chem. Phys.* **142** 034107
- [48] Perdew J P, Ernzerhof M and Burke K 1996 *J. Chem. Phys.* **105** 9982
- [49] Ernzerhof M, Perdew J P and Burke K 1997 *Int. J. Quantum Chem.* **64** 285
- [50] Lutterotti L and Scardi P 1990 *J. Appl. Crystallogr.* **23** 246
- [51] French R H 1990 *J. Am. Ceram. Soc.* **73** 477
- [52] Cox R 1971 *Solid State Commun.* **9** 1989
- [53] Duvarney R C, Niklas J R and Spaeth J M 1985 *Phys. Status Solidi b* **128** 673
- [54] Wang H, Lee C and Kröger F 1983 *Phys. Rev. B* **27** 3821
- [55] Adrian F J, Jette A N and Spaeth J M 1985 *Phys. Rev. B* **31** 3923
- [56] Iannuzzi M, Chassaing T, Wallman T and Hutter J 2005 *CHIMIA Int. J. Chem.* **59** 499–503
- [57] Groner M D, Fabreguette F H, Elam J W and George S M 2004 *Chem. Mater.* **16** 639
- [58] Ilic B, Krylov S and Craighead H G 2010 *J. Appl. Phys.* **108** 044317
- [59] Lamparter P and Kniep R 1997 *Physica B* **236** 405
- [60] Lee S, Park S, Yi Y and Ahn C 2009 *Phys. Rev. Lett.* **103** 095501
- [61] Afanas'ev V V, Stesmans A and Tsai W 2003 *Appl. Phys. Lett.* **82** 245
- [62] Huang M L, Chang Y C, Chang C H, Lin T D, Kwo J, Wu T B and Hong M 2006 *Appl. Phys. Lett.* **89** 012903
- [63] Nguyen N V *et al* 2008 *Appl. Phys. Lett.* **93** 082105

- [64] Ahn J, Geppert I, Gunji M, Holland M, Thayne I, Eizenberg M and McIntyre P C 2011 *Appl. Phys. Lett.* **99** 23
- [65] Krylov I, Ritter D and Eizenberg M 2015 *J. Appl. Phys.* **117** 174501
- [66] Bell R and Dean P 1971 *Discuss. Faraday Soc.* **1970** 55
- [67] Chang T M, Bauer J D and Skinner J L 1990 *J. Chem. Phys.* **93** 8973
- [68] Dong J and Drabold D 1996 *Phys. Rev. B* **54** 10284
- [69] Unge M and Christen T 2014 *Chem. Phys. Lett.* **613** 15
- [70] Youn Y, Kang Y and Han S 2014 *Comput. Mater. Sci.* **95** 256
- [71] Mott N 1987 *J. Phys. C: Solid State Phys.* **3075** 3075
- [72] Dong J and Drabold D 1998 *Phys. Rev. Lett.* **80** 1928
- [73] Sabino F P, Besse R, Oliveira L N, Wei S H and Da Silva J L F 2015 *Phys. Rev. B* **92** 205308
- [74] Boykin T B, Kharche N, Klimeck G and Korkusinski M 2007 *J. Phys.: Condens. Matter* **19** 036203
- [75] Chang C-Y, Pan F-M, Lin J-S, Yu T-Y, Li Y-M and Chen C-Y 2016 *J. Appl. Phys.* **120** 234501